Microporous and Mesoporous Materials 204 (2015) 1–7

Contents lists available at ScienceDirect

Microporous and Mesoporous Materials

journal homepage: www.elsevier.com/locate/micromeso

Imidazolium-based ionic liquids as novel organic SDA to synthesize high-silica Y zeolite

Danhua Yuan [a,b,c], Dawei He [a,b,c], Shutao Xu [a,b], Zhijia Song [a,b,c], Mozhi Zhang [a,b,c], Yingxu Wei [a,b], Yanli He [a,b], Shuliang Xu [a,b], Zhongmin Liu [a,b,*], Yunpeng Xu [a,b,*]

[a] National Engineering Laboratory for Methanol to Olefins, Dalian Institute of Chemical Physics, Chinese Academy of Sciences, P.O. Box 110, 116023 Dalian, PR China
[b] Dalian National Laboratory for Clean Energy, Dalian Institute of Chemical Physics, Chinese Academy of Sciences, Dalian, PR China
[c] Graduate University of Chinese Academy of Sciences, Beijing 100049, PR China

ARTICLE INFO

Article history:
Received 3 June 2014
Received in revised form 20 October 2014
Accepted 30 October 2014
Available online 8 November 2014

Keywords:
Y zeolite
High silica
Ionic liquid
Synthesis

ABSTRACT

Alkyl-substituted imidazolium-based ionic liquid as a novel type of organic structure-directing agent (SDA) was employed to synthesize high-silica Y zeolite with a SiO_2/Al_2O_3 ratio of approximately 6.20–6.40. The XRD, SEM, BET and ^{27}Al NMR characterizations showed that the products synthesized with the ionic liquids 1-ethyl-3-methylimidazolium bromide or 1-butyl-3-methylimidazolium bromide were highly crystalline pure phase Y zeolite. Moreover, the TG, TOC, XRF and ^{13}C NMR results suggested that 1-ethyl-3-methylimidazolium or 1-butyl-3-methylimidazolium cations were trapped within the pores of the faujasite structure and played the role of structure-directing agents. 1-Ethyl-3-methylimidazolium and 1-butyl-3-methylimidazolium cations can partially replace the sodium cations to balance the negative charges of the zeolite framework, which facilitated the formation of a high SiO_2/Al_2O_3 ratio faujasite structure.

1. Introduction

FAU type zeolite (faujasite) with a super-cage structure is classified as X- and Y-type zeolite according to the silica-to-alumina ratio [1]. X-type zeolite with a SiO_2/Al_2O_3 ratio of 2.2–3 has been used as an important adsorbent for gas separation and cleaning [2,3]. Y-type zeolite with a SiO_2/Al_2O_3 ratio of 3–5 has been widely used as a catalyst for oil refining, particularly for fluid catalytic cracking (FCC) processes [4–7]. Zeolite Y is the active component of the catalytic cracking catalyst, and its catalytic performance is mainly dependent on its framework SiO_2/Al_2O_3 ratio [8–10]. An increase in the framework SiO_2/Al_2O_3 ratio in zeolite Y improves its activity and thermal-hydrothermal stability [9,11]. Therefore, the preparation of Y zeolite with a high silica-to-alumina ratio has attracted significant attention.

At present, classical synthesis allows the preparation of Y zeolite with a SiO_2/Al_2O_3 molar ratio of only approximately 5.4 [9]. The high-silica Y zeolite used in FCC catalysts in industry is mainly from post-treatment procedures, which comprise the extraction of aluminum and complement of silicon to improve the secondary synthetic silica-to-alumina ratio [12,13]. However, the post-treatment procedures have many drawbacks, such as complicated preparation steps, considerable loss of zeolite crystallinity, and serious environmental pollution. The direct synthesis of high-silica Y zeolite ($SiO_2/Al_2O_3 > 6$) is difficult but it is possible to avoid the complicated post-treatment processes, preserve high zeolite crystallinity and reduce environmental pollution. In addition, the directly synthesized high-silica Y zeolite ($SiO_2/Al_2O_3 > 6$) exhibits outstanding catalytic activity due to its complete crystal structure and uniform chemical distribution [14,15].

The direct synthesis of high-silica Y zeolite ($SiO_2/Al_2O_3 > 6$) can be achieved using organic SDAs. Initially, a high-silica faujasite polymorph with a SiO_2/Al_2O_3 ratio greater than 6, similarly to CSZ-3, ECR-4 and ECR-32, was prepared with cesium ion, bis-(2-hydroxyethyl)-dimethylammonium ions and tetrapropyl ammonium and/or tetrabutyl ammonium trapped within the pores of the faujasite structure [16–18]. Delprato et al. first prepared high-crystallinity Y zeolite with a SiO_2/Al_2O_3 ratio of 9 using 15-crown-5 as the SDA [19]. After that, many efforts were devoted to the use of crown ether as the SDA to synthesize high-silica Y zeolite [20–24]. Crown ether has been considered the best organic SDA to date for the synthesis of high-silica Y zeolite, but its high cost and toxicity have restricted its industrial application. Zeolite

* Corresponding authors at: National Engineering Laboratory for Methanol to Olefins, Dalian Institute of Chemical Physics, Chinese Academy of Sciences, P.O. Box 110, 116023 Dalian, PR China. Tel./fax: +86 0411 84379518.
E-mail addresses: liuzm@dicp.ac.cn (Z. Liu), xuyp@dicp.ac.cn (Y. Xu).

http://dx.doi.org/10.1016/j.micromeso.2014.10.049
1387-1811/

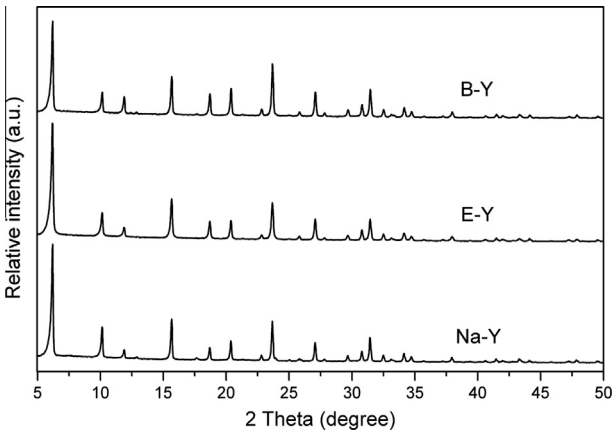

Fig. 1. XRD patterns of the as-synthesized samples E-Y, B-Y, and Na-Y.

Y with a framework SiO_2/Al_2O_3 ratio of 6.8 could also be obtained using tris(3,6-dioxaheptyl)amine (TDA-1) and poly(ethylene oxides) (PEO), which are acyclic molecules containing ($-OCH_2CH_2-$) groups [25]. Witte et al. prepared high-silica Y zeolite with a SiO_2/Al_2O_3 ratio of 6.2 by employing inositol as the organic SDA [26]. Recently, Xiao et al. obtained high-silica Y zeolite ($SiO_2/Al_2O_3 > 6$) with good crystallinity in the presence of N-methylpyridinium iodide and demonstrated that high-silica Y zeolite exhibits good catalytic performance and excellent adsorptive properties [15]. Dozens of structure-directing agents have been employed to synthesize high-silica Y zeolite, mainly including cesium ion, quaternary ammonium hydroxide, crown ether, and linear and cyclic alcohols. Amongst the various SDAs, quaternary ammonium hydroxide is the most commonly used, crown ether is considered to be the best organic SDAs, and organic SDAs of nitrogen-containing heterocyclic compounds are a new system for synthesizing high-silica Y zeolite.

Ionic liquids have been recently explored for the synthesis of molecular sieves; they are not only green solvents but also act as structure-directing agents in zeolite synthesis, such as MCM-41 [27], ZSM-5 and beta zeolites [28]. In the present work, imidazolium-based ionic liquids were employed as the organic SDAs to synthesize high-silica Y zeolite, and highly crystalline Y zeolite with SiO_2/Al_2O_3 ratios greater than 6 were successfully obtained in the experiments. The zeolite samples were characterized by X-ray diffraction (XRD), X-ray fluorescence (XRF), scanning electron microscopy (SEM), low-temperature N_2 adsorption/desorption analysis, thermogravimetry analysis (TG) and nuclear magnetic resonance (NMR). A possible mechanism for high-silica Y zeolite formation with the aid of imidazolium-based ionic liquid SDAs is also discussed in this manuscript.

2. Experimental section

2.1. Synthesis

The chemical reagents used in the experiments included silica sol (SiO_2 = 30%, Na_2O = 0.25%, Qingdao Ocean Chemical Plant), $NaAlO_2$ (Al_2O_3 = 48%, Na_2O = 40%, Sinopharm Chemical Reagent Corp.), NaOH (98%, Tianjin Kemiou Chemical Reagent Corp.), 1-ethyl-3-methylimidazolium bromide [EMIm]Br and 1-butyl-3-methylimidazolium bromide [BMIm]Br (99%, Shanghai Dibo Chemical Reagent Corp.). All of the above reagents were used without further purification.

The process of synthesizing high-silica Y zeolite was as follows: first, 3.60 g of 1-ethyl-3-methylimidazolium bromide, 2 g of $NaAlO_2$ and 2.15 g of NaOH were added into 33 g of deionized water with stirring to form a clear solution. Next, 24.47 g of silica sol was mixed with the above clear solution with strong agitation to obtain the final gel with a molar composition of $1Al_2O_3$: $13SiO_2$:2[EMIm]Br:$3.92Na_2O$:$300H_2O$. This mixture was aged for 12 h with agitation, was then transferred into a stainless steel autoclave, and placed in an oven statically at 100 °C for a certain time. After crystallization, the powdered products were separated by filtration, washed with deionized water until pH < 8, and then dried at 100 °C for further characterization. The samples synthesized with [EMIm]Br and [BMIm]Br as the organic SDAs at 100 °C for 14 days were named E-Y and B-Y, respectively, and the sample obtained from the same aluminosilicate gel without an organic SDA was named Na-Y. The crystallization kinetic curve of Y zeolite was plotted against the relative crystallinity, which was calculated from the reflections at 2 theta = 6.2°, 15.7° and 23.7° corresponding to the (hkl)-values of (1 1 1), (3 3 1) and (5 3 3), respectively. The sample crystallized for 14 days with the intensities of the 1 1 1, 3 3 1, and 5 3 3 planes reaching the maximum was defined as completely (100%) crystalline. For further BET measurement, calcination was conducted at 500 °C for 2 h to remove water and organic species.

2.2. Characterization

The synthesized products were characterized using X-ray powder diffraction (XRD) for phase identification. The X-ray diffraction patterns were recorded with a PANalytical X'Pert PRO X-ray

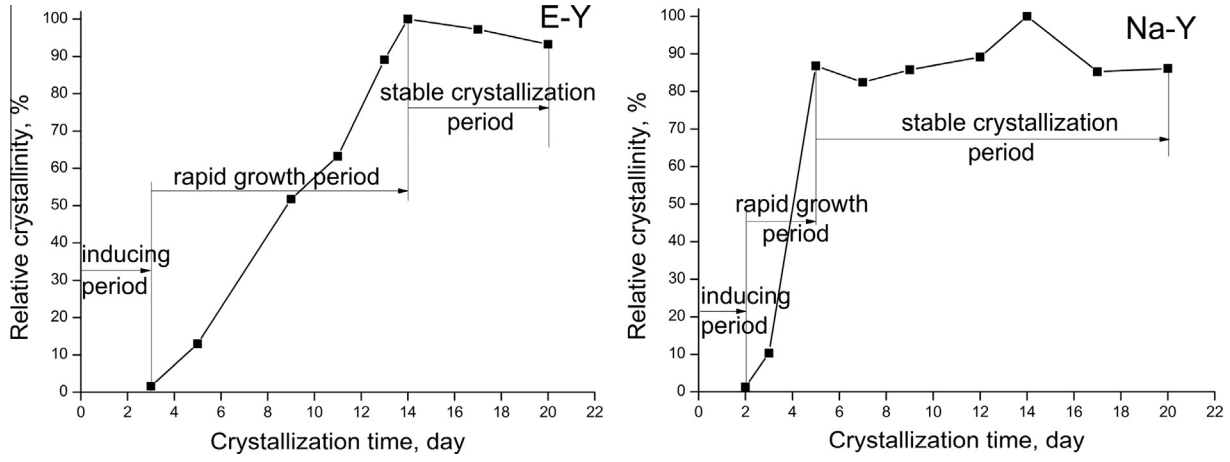

Fig. 2. Crystallization kinetic curves of the as-synthesized samples E-Y and Na-Y.

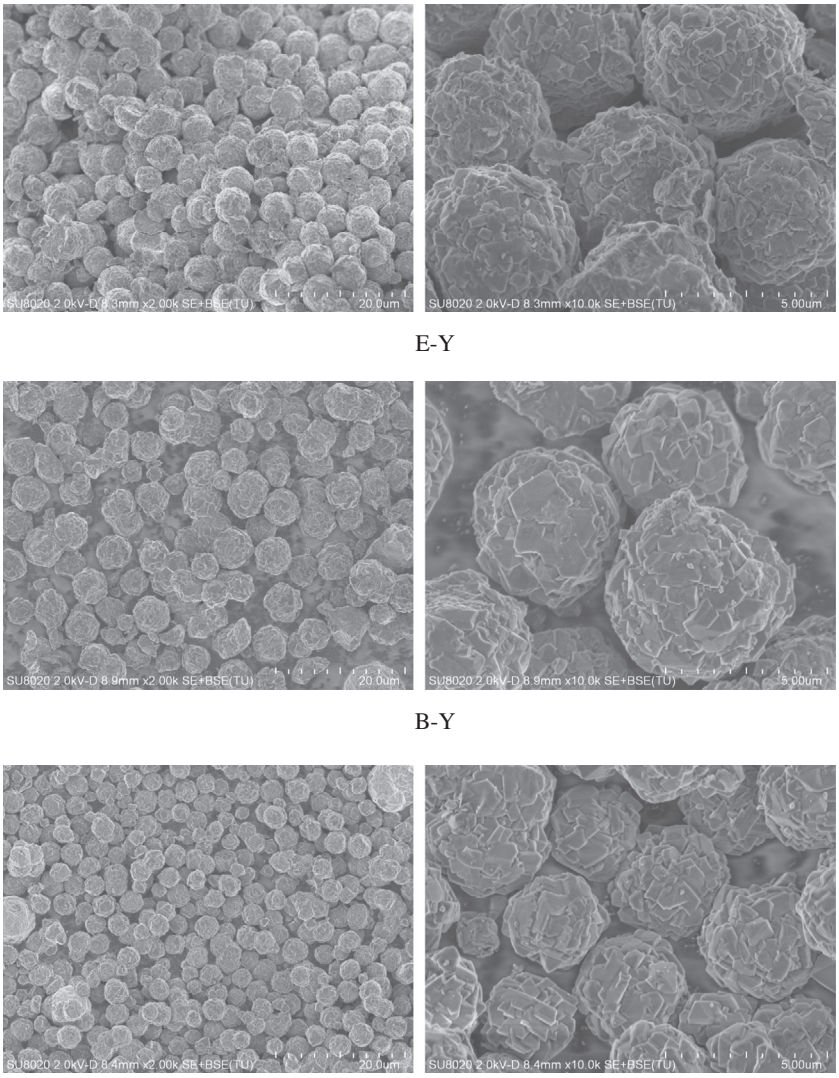

Fig. 3. SEM images of the as-synthesized samples E-Y, B-Y, and Na-Y.

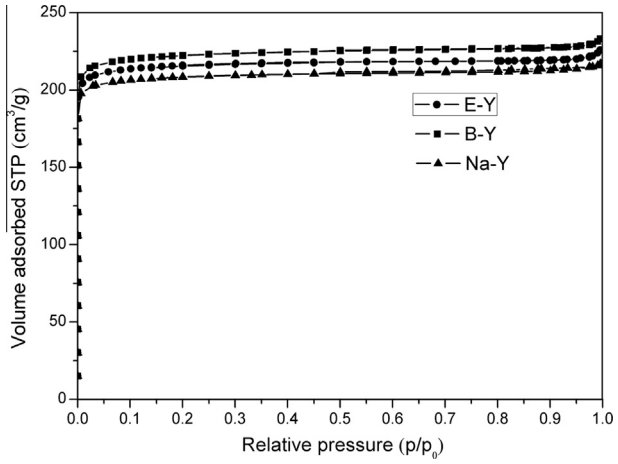

Fig. 4. N_2 adsorption–desorption isotherms of the as-synthesized samples E-Y, B-Y and Na-Y.

Table 1
Textural properties of samples E-Y, B-Y, and Na-Y.

Sample	Surface area (m^2/g)			Pore volume (cm^3/g)	
	S_{total} [a]	S_{micro} [b]	S_{ext} [c]	V_{total}	V_{micro} [d]
E-Y	723	673	49	0.34	0.31
B-Y	741	687	54	0.35	0.32
Na-Y	694	650	43	0.33	0.30

[a] BET surface area.
[b] *t*-Plot micropore surface area.
[c] *t*-Plot external surface area.
[d] *t*-Plot micropore volume.

diffractometer using Cu-Kα radiation (λ = 1.54059 Å) operating at 40 kV and 40 mA. The chemical composition of the solid samples was determined with a Philips Magix-601 X-ray fluorescence (XRF) spectrometer. The crystal size and morphology were investigated using a Hitachi SU8020 scanning electron microscope. All of the solid-state NMR experiments were performed on a Bruker

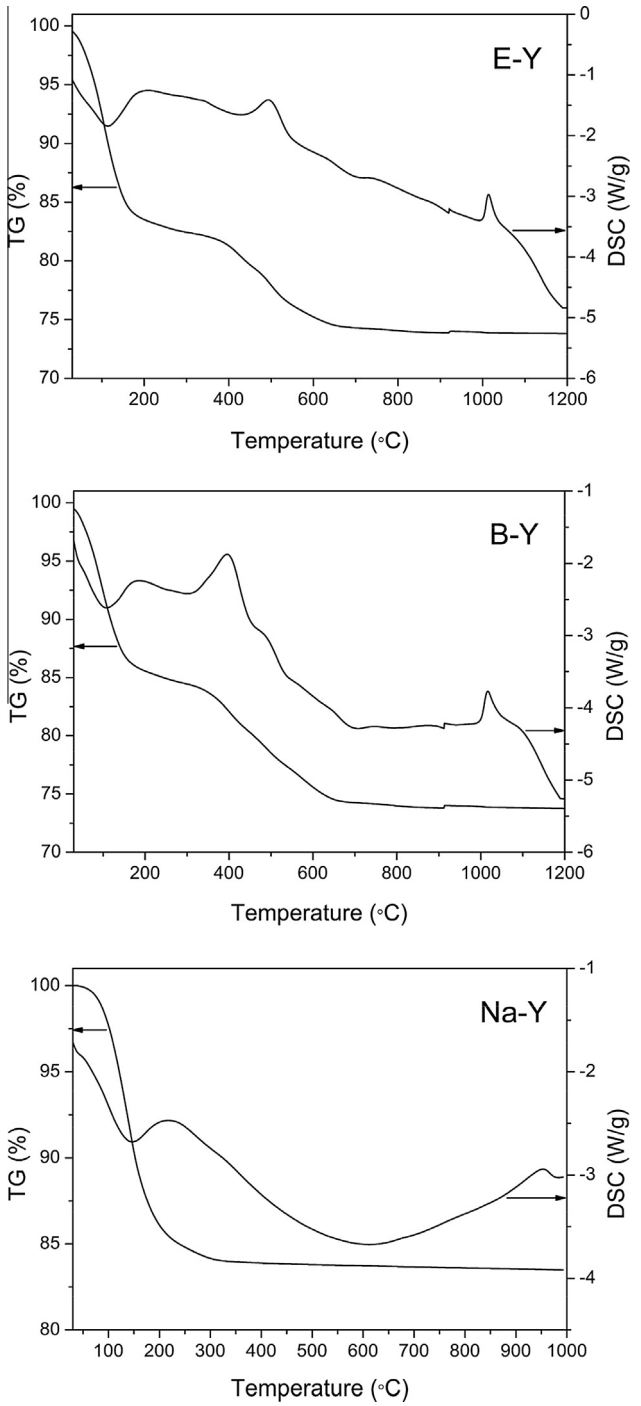

Fig. 5. TG and DSC curves of the as-synthesized samples E-Y, B-Y and Na-Y.

Table 2
The TG weight loss and carbon content in the as-synthesized Y zeolites.

Sample	TG weight loss (%)		Carbon content in zeolite (%)	
	(<300 °C)	(300–700 °C)	TOC[a]	TG[b]
E-Y	17.12	8.14	5.73	6.08
B-Y	15.04	10.18	7.51	8.12
Na-Y	15.84	0.49	–	–

[a] Carbon content obtained from TOC.
[b] Carbon content obtained from TG.

AvanceIII 600 spectrometer equipped with a 14.1 T wide-bore magnet. The resonance frequencies were 156.4 and 119.2 MHz for ^{27}Al and ^{29}Si, respectively. ^{27}Al MAS NMR experiments were performed on a 4-mm MAS probe with a spinning rate of 12 kHz. The ^{27}Al MAS NMR spectra were recorded using a one pulse sequence. A total of 600 scans were accumulated with a $\pi/8$ pulse width of 0.75 μs and a 2-s recycle delay. The chemical shifts were referenced to $(NH_4)Al(SO_4)_2{\cdot}12H_2O$ at −0.4 ppm. The ^{29}Si MAS NMR spectra were recorded with a 7-mm MAS probe with a spinning rate of 6 kHz using high-power proton decoupling. A total of 1024 scans were accumulated with a $\pi/4$ pulse width of 2.5 μs and a 10 s recycle delay. The chemical shifts were referenced to 4,4-dimethyl-4-silapentane sulfonate sodium salt (DSS). The ^{13}C liquid NMR spectra were performed on a Bruker AvanceIII 400 spectrometer equipped with a 9.4 T narrow-bore magnet, and the resonance frequency was 150.9 MHz. The deuterium solvent was D_2O, and the chemical shifts were referenced to tetramethylsilane (TMS) at 0 ppm. The textural properties of the calcined samples were determined by N_2 adsorption–desorption isotherms at 77 K on a Micromeritics ASAP 2020 system. The total surface area was calculated based on the BET equation, and the micropore surface area was evaluated using the *t*-plot method. The thermogravimetry analysis was performed on a TA Q-600 analyzer. The samples were heated from room temperature to 1200 °C at a heating rate of 10 °C/min with an air flow of 100 ml/min. The contents of water and template in the as-synthesized samples were calculated according to the weight losses at temperatures lower than 300 °C and in the range of 300–700 °C in the TG curve, respectively. The total carbon content in the residue (coke/char) after the reactions was determined using an instrument for total organic carbon analysis (Shimadzu TOC-L CPH) with a solid sample module (SSM-5000A). The temperature of the total carbon combustion tube of the SSM-5000A was 900 °C. Approximately 50 mg of solid sample was loaded in a ceramic sample boat and analyzed by further combustion.

3. Results and discussion

The XRD patterns shown in Fig. 1 indicated that samples E-Y, B-Y and Na-Y were highly crystalline Y zeolite without any detectable impurities, regardless of whether the synthesis gel contained [E(B)MIm]Br. The crystallization kinetic curves of samples E-Y and Na-Y, which are shown in Fig. 2, were used to evaluate the crystallization process with or without an organic SDA. Both of the crystallization curves exhibited typical S-shaped curves, which indicated that the crystallization process of Y zeolite comprised an inducing period, a continuous growth period and a stable crystallization period. However, the inducing period of sample Na-Y (0–2 days) was slightly shorter than that of sample E-Y (0–3 days), and the growth period of sample Na-Y (2–5 days) was also shorter than that of sample E-Y (3–14 days), which indicated that the processes of spontaneous nucleation and growth were easier in the absence of [EMIm]Br.

The SEM micrographs (Fig. 3) show that E-Y, B-Y and Na-Y displayed similar spherical agglomerates, but the average crystal size of NaY was approximately 3–4 μm, which is much smaller than that of E-Y and B-Y (5–6 μm). The particle size was largely affected by the amount of nuclei formed during the inducing period; a large amount of nuclei resulted in small zeolite crystals [29]. Therefore, the reduction in the particle size of sample Na-Y was consistent with the shortening of the inducing period of sample Na-Y, as displayed in Fig. 2. The ^{27}Al MAS-NMR results of samples E-Y, B-Y and Na-Y showed similar behavior, only a peak at 60 ppm was assigned to tetrahedrally coordinated framework aluminum species. The

Table 3
Gel compositions, crystallization conditions and SiO_2/Al_2O_3 ratios of the as-synthesized Y zeolites.

Sample	$Na_2O/Al_2O_3/SiO_2/H_2O$/[E(B)MIm]Br	Crystallization time (day)	Crystal phase	SiO_2/Al_2O_3 ratio of products	
				^{29}Si NMR[a]	XRF[b]
E-Y	3.92/1/13/300/2	14	Y	6.24	6.40
B-Y	3.92/1/13/300/2	14	Y	6.20	6.32
Na-Y	3.92/1/13/300/0	14	Y	5.64	5.78
B-Y-1	3.92/1/13/300/1	14	Y + Amor	–	–
B-Y-2	3.92/1/13/300/4	14	Y + Amor	–	–
B-Y-3	4.92/1/13/300/2	7	Y	–	4.96
B-Y-4	3.65/1/13/300/2	14	Y + Amor	–	–
B-Y-5	3.40/1/13/300/2	14	Amor	–	–

[a] SiO_2/Al_2O_3 ratios obtained from ^{29}Si NMR.
[b] SiO_2/Al_2O_3 ratios obtained from XRF.

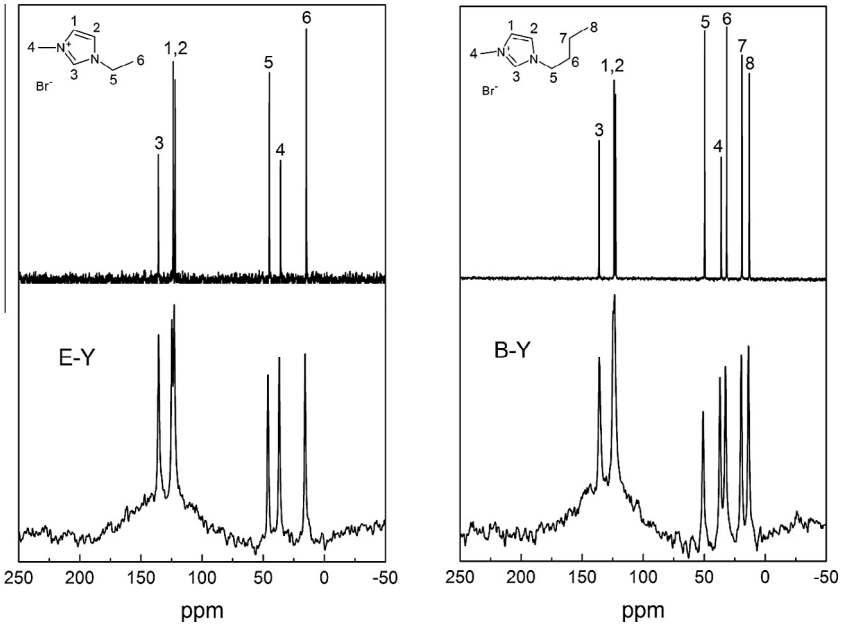

Fig. 6. ^{13}C NMR spectra of the as-synthesized samples E-Y and B-Y.

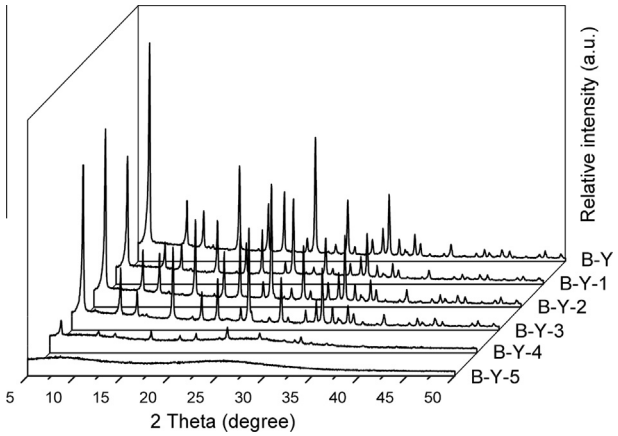

Fig. 7. XRD patterns of the as-synthesized samples B-Y and B-Y-(1–5).

textural properties of the calcined samples were characterized by nitrogen physical adsorption, and the isotherms of samples E-Y, B-Y and Na-Y are shown in Fig. 4. These samples displayed a similar typical type I isotherm with the characteristic of microporous materials. The specific surface areas and the pore volumes of these samples are listed in Table 1. The lack of hysteresis loop between the adsorption and desorption branches of the isotherms confirmed the absence of extensive mesopores in these materials, which was in accordance with the small external surface area of the samples (Table 1). The BET specific surface area of samples E-Y and B-Y were 723 and 741 m^2/g, respectively, which are slightly larger than that (694 m^2/g) of sample Na-Y. The rich BET specific surface area and micropore volume demonstrated that all of the samples were highly crystallized and contained a considerable amount of micropores in the zeolite framework. All of these characterizations proved that highly crystalline Y zeolite without any detectable impurities could be synthesized in the presence of [E(B)MIm]Br. In addition, the nucleation and growth rate of sample E-Y were less than those of sample Na-Y, which led to the formation of relatively large zeolite crystals in sample E-Y synthesized with [EMIm]Br.

The TG/DSC curves of samples E-Y, B-Y and Na-Y are shown in Fig. 5, and the corresponding weight losses of each stage of the zeolite formation process are listed in Table 2. The weight loss with an endothermic effect in the temperature range of 100–300 °C was due to water desorption from the zeolites. The samples E-Y, B-Y and Na-Y contained approximately 17.12%, 15.04% and 15.84%

water at 300 °C, respectively. For samples E-Y and B-Y, the weight losses with an exothermic effect in the temperature range of 300–700 °C were attributed to the removal of organic templates, and the weight losses of the organic template removal from samples E-Y and B-Y were 8.14% and 10.18%, respectively. However, for sample Na-Y, which was synthesized without the organic template, there was no obvious exothermic effect in the temperature range of 300–700 °C, and the weight loss of 0.49% observed in this temperature range might be attributed to the dehydration of structural defects, such as terminal OH groups (silanol), in the zeolite framework [30]. The exothermic peaks at the high temperature range from 900 °C to 1100 °C without weight change were attributed to the structural collapse of the zeolite framework, which could indicate the thermal stability of Y zeolite [31]. The high temperature exothermic peaks of samples E-Y, B-Y and Na-Y appeared at different temperatures, such as 950 °C for sample Na-Y and at a higher temperature (1020 °C) for samples E-Y and B-Y, which indicated that Y zeolite synthesized with [E(B)MIm]Br displayed higher thermal stability. The improved thermal stability was in good agreement with the relatively high SiO_2/Al_2O_3 ratio (Table 3). The detailed carbon contents in the zeolite samples are also listed in Table 2. Both TOC and TG methods were used to calculate the carbon contents in the zeolite samples. For sample E-Y, the carbon contents calculated by the TOC and TG methods were 5.73% and 6.08%, respectively, and for sample B-Y, the carbon contents were 7.51% and 8.12%, respectively, which indicated that there was a certain amount of organic template present in samples E-Y and B-Y. Fig. 6 shows the ^{13}C NMR spectra of 1-ethyl-3-methylimidazolium bromide and sample E-Y and of 1-butyl-3-methylimidazolium bromide and sample B-Y. The peaks at 122.8 ppm, 124.7 ppm and 135.6 ppm were assigned to three carbon environments in the imidazole ring, and the resonance peak at 36.9 ppm represented the N-CH_3 group of the imidazole ring. For sample E-Y and 1-ethyl-3-methylimidazolium bromide, the signals at 15.8 ppm and 46.2 ppm were related to the two carbon environments of the N-CH_2-CH_3 group in the 1-ethyl-3-methylimidazolium cations. For sample B-Y and 1-butyl-3-methylimidazolium bromide, the signals at 13.7 ppm, 19.6 ppm, 32.6 ppm and 50.9 ppm were assigned to the four carbon environments of the N-CH_2-CH_2-CH_2-CH_3 group in the 1-butyl-3-methylimidazolium cations. The ^{13}C NMR results implied that the [E(B)MIm] cations were stable in samples E-Y and B-Y. Furthermore, the Na_2O/Al_2O_3 ratios measured from the XRF of samples E-Y and B-Y were 0.71 and 0.70, respectively, which are lower than that of sample Na-Y, which has a Na_2O/Al_2O_3 ratio of 0.98. The XRF result suggested that the [E(B)MIm] cations can partially replace the sodium cations to balance the negative charges of the zeolite framework [15], which was consistent with the ^{13}C NMR, TG and TOC results. All of these results demonstrated that the [E(B)MIm] cations, as stable SDAs, were incorporated in the pores of Y zeolite and partially replaced the sodium cations to balance the negative charges of the zeolite framework.

The detailed compositions of the starting gels, crystallization conditions and SiO_2/Al_2O_3 ratios of the products are presented in Table 3, and the corresponding XRD patterns of these samples are shown in Fig. 7. ^{29}Si NMR and XRF were used to investigate the SiO_2/Al_2O_3 ratio of the products, and samples E-Y and B-Y showed similar SiO_2/Al_2O_3 ratios of approximately 6.20–6.40. The SiO_2/Al_2O_3 ratio of sample Na-Y (5.64) was significantly lower than those of samples E-Y (6.24) and B-Y (6.20), which could be explained by the relatively large organic cations ($[E(B)MIm]^+$) introducing a lower number of positive charges than small inorganic cations (Na^+) within the zeolite cages, thus requiring a lower number of framework Al to balance the positive charges [32]. Fig. 8 shows the ^{29}Si NMR spectra of the as-synthesized samples E-Y, B-Y and Na-Y; the signals of Si(0Al) and Si(1Al) species in

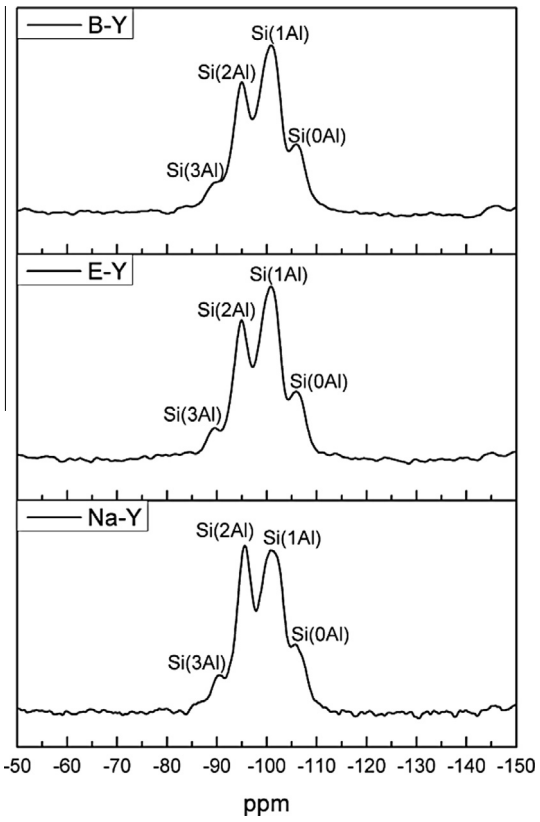

Fig. 8. ^{29}Si NMR spectra of the as-synthesized samples E-Y, B-Y and Na-Y.

samples E-Y and B-Y were significantly enhanced compared with those of sample Na-Y, whereas the signal of the Si(2Al) species was weakened, which resulted in improvement of the framework SiO_2/Al_2O_3 ratio in samples E-Y and B-Y. These results demonstrated that a higher SiO_2/Al_2O_3 ratio could be obtained in the presence of organic SDAs ([E(B)MIm]Br). Then, the influence of the amount of [BMIm]Br in the crystallization of a typical FAU synthesis gel was investigated. By reducing the [BMIm]Br/Al_2O_3 ratio to 1 or increasing the ratio to 4 in the gel, an amorphous phase appeared, accompanied by Y zeolite after crystallization for 14 days, which indicated that the type of crystallization did not change by varying the amount of organic SDA, but longer crystallization times were required. With an increase in the Na_2O content in the gel, the crystallization rate of zeolite accelerated, but the SiO_2/Al_2O_3 molar ratio in the framework decreased. Similarly to samples B-Y and B-Y-3, an increase in the Na_2O/Al_2O_3 ratio from 3.92 to 4.92 decreased the fully crystallized time from 14 days to 7 days, and the SiO_2/Al_2O_3 molar ratio in the framework decreased from 6.32 to 4.96. In contrast, when the Na_2O content was decreased in the gel, the crystallization rate of zeolite was decreased, as was observed with sample B-Y and sample B-Y-4. A decrease in the Na_2O/Al_2O_3 ratio from 3.92 to 3.65 resulted in the appearance of an amorphous phase, accompanied by Y zeolite in sample B-Y-4 under the same crystallization time. After further decreasing the Na_2O/Al_2O_3 ratio to 3.40, an amorphous phase was obtained as the sole phase, just as in sample B-Y-5. These results suggested that the crystallization rate of Y zeolite was decreased, and the amorphous phase emerged when organic [BMIm]Br was applied in too great or too small a quantity, whereas the crystallization rate was accelerated and the SiO_2/Al_2O_3 molar ratio was decreased when the Na_2O content was increased in the gel. Therefore, the gel composition required to crystallize high-silica Y was within a rather narrow range.

4. Conclusion

High-silica Y zeolite was successfully synthesized using [E(B)MIm]Br as a novel organic SDA. The XRD, SEM and ^{27}Al MAS-NMR results showed that highly crystalline Y zeolite without any detectable impurities could be synthesized in the presence of [E(B)MIm]Br. The crystallization kinetic curves showed that the inducing period was extended by adding [EMIm]Br to the synthesis gel. The ^{13}C NMR, TG, TOC and XRF results demonstrated that the [E(B)MIm] cations, as stable SDAs, were incorporated into the pores of Y zeolite and partially replaced the sodium cations to balance the negative charges of the zeolite framework. ^{29}Si NMR and XRF were used to investigate the SiO_2/Al_2O_3 ratio of the products, and the samples synthesized with [E(B)MIm]Br displayed higher SiO_2/Al_2O_3 ratios of approximately 6.20–6.40, which was consistent with their higher thermal stability. In addition, we investigated the influences of the crystallization conditions and gel compositions on the SiO_2/Al_2O_3 molar ratio and found that the contents of organic SDAs ([E(B)MIm]Br) and Na_2O in the starting gel were within a narrow range for crystallizing high-silica Y zeolite.

References

[1] T. Frising, P. Leflaive, Microporous Mesoporous Mater. 114 (2008) 27–63.
[2] J.S. Lee, J.H. Kim, J.T. Kim, J.K. Suh, J.M. Lee, C.H. Lee, J. Chem. Eng. Data 47 (2002) 1237–1242.
[3] V.P. Mulgundmath, F.H. Tezel, T. Saatcioglu, T.C. Golden, Can. J. Chem. Eng. 90 (2012) 730–738.
[4] S. Magyar, J. Hancsok, D. Kallo, Fuel Process. Technol. 86 (2005) 1151–1164.
[5] A. Corma, G.W. Huber, L. Sauvanaud, P. O'Connor, J. Catal. 247 (2007) 307–327.
[6] S. Al-Khattaf, N.M. Tukur, A. Al-Amer, U.A. Al-Mubaiyedh, Appl. Catal. A Gen. 305 (2006) 21–31.
[7] M.A. Sanchez-Castillo, N. Agarwal, C. Miller, R.D. Cortright, R.J. Madon, J.A. Dumesic, J. Catal. 205 (2002) 67–85.
[8] R.A. Beyerlein, G.B. McVicker, L.N. Yacullo, J.J. Ziemiak, J. Phys. Chem. 92 (1988) 1967–1970.
[9] J. Scherzer, Appl. Catal. 75 (1991) 1–32.
[10] J. Dwyer, K. Karim, W.J. Smith, N.E. Thompson, R.K. Harris, D.C. Apperley, J. Phys. Chem. 95 (1991) 8826–8831.
[11] M.A. Camblor, A. Corma, A. Martínez, F.A. Mocholí, J.P. Pariente, Appl. Catal. 55 (1989) 65–74.
[12] G.T. Kerr, J. Phys. Chem. 72 (1968) 2594–2596.
[13] H.K. Beyer, I. Belenykaja, Stud. Surf. Sci. Catal. Elsevier (1980) 203–210.
[14] B. Xu, S. Bordiga, R. Prins, J.A. van Bokhoven, Appl. Catal. A Gen. 333 (2007) 245–253.
[15] L. Zhu, L. Ren, S. Zeng, C. Yang, H. Zhang, X. Meng, M. Rigutto, A. van der Made, F.-S. Xiao, Chem. Commun. 49 (2013) 10495–10497.
[16] M.G. Barrett, D.E. Vaughan, U.S. Patent 4333,859, 1982.
[17] D.E. Vaughan, U.S. Patent 4714,601, 1987.
[18] K.G. Strohmaier, D.E. Vaughan, U.S. Patent 4931,267, 1990.
[19] F. Delprato, L. Delmotte, J.L. Guth, L. Huve, Zeolites 10 (1990) 546–552.
[20] J.P. Arhancet, M.E. Davis, Chem. Mater. 3 (1991) 567–569.
[21] S.L. Burkett, M.E. Davis, Microporous Mater. 1 (1993) 265–282.
[22] E.J.P. Feijen, K. Devadder, M.H. Bosschaerts, J.L. Lievens, J.A. Martens, P.J. Grobet, P.A. Jacobs, J. Am. Chem. Soc. 116 (1994) 2950–2957.
[23] C.N. Wu, K.J. Chao, J. Chem. Soc., Faraday Trans. 91 (1995) 167–173.
[24] K. Karim, J. Zhao, D. Rawlence, J. Dwyer, Microporous Mater. 3 (1995) 695–698.
[25] F. Dougnier, J. Patarin, J.L. Guth, D. Anglerot, Zeolites 13 (1993) 122–127.
[26] B. De Witte, J. Patarin, D. Le Nouen, L. Delmotte, J.L. Guth, T. Cholley, Microporous Mesoporous Mater. 23 (1998) 11–22.
[27] C.J. Adams, A.E. Bradley, K.R. Seddon, Aust. J. Chem. 54 (2001) 679–681.
[28] M.L. Mignoni, M.O. de Souza, S.B.C. Pergher, R.F. de Souza, K. Bernardo-Gusmao, Appl. Catal. A Gen. 374 (2010) 26–30.
[29] C. Berger, R. Glaser, R.A. Rakoczy, J. Weitkamp, Microporous Mesoporous Mater. 83 (2005) 333–344.
[30] H. Zhang, B. Xie, X. Meng, U. Müller, B. Yilmaz, M. Feyen, S. Maurer, H. Gies, T. Tatsumi, X. Bao, W. Zhang, D. De Vos, F.-S. Xiao, Microporous Mesoporous Mater. 180 (2013) 123–129.
[31] A.W. Coats, J.P. Redfern, Nature 201 (1964) 68–69.
[32] M. Moliner, F. Rey, A. Corma, Angew. Chem. Int. Ed. 52 (2013) 13880–13889.